

1 **Neogene-Recent Reactivation of Jurassic-age Faults in Southern Vietnam, with Implications for the**  
2 **Extrusion of Indochina**

3 Authors: CM Burberry, LJ Elkins, Nguyen Hoang, Le Duc Anh, Sang Q. Dinh.

4 Affiliations: UNL, VAST, Petrovietnam University

5

6 **ABSTRACT**

7 Onshore Vietnam contains a complex series of faults coupled with a diffuse igneous province that has  
8 been active since the mid-Miocene. However, there are several conflicting fault maps in the literature and  
9 no consensus concerning the relative age of mapped faults and Neogene basalt flows, which becomes  
10 problematic when trying to use structural data to distinguish between competing tectonic models for the  
11 SE Asia region. This paper aims to define the Neogene-Recent tectonic setting and kinematics of the Da  
12 Lat block of the onshore Vietnam region, by analyzing the orientation, kinematics and ages of faults across  
13 a sub-region of the block. Fault ages can be constrained by the cross-cutting relationships with dated  
14 basalt flows. Results from remote sensing show a strong NE-SW fault trend for southern Vietnam, with  
15 additional, minor N-S, E-W and NW-SE trends. Fault orientations observed in the field fall into this NE-SW  
16 trending class, and are sub-vertical. In the basalt flows (with eruption ages < 5 Ma) these faults have  
17 oblique lineations with a strong strike-slip component. In Jurassic sediments, these faults show two sets  
18 of lineations: an older, dip-slip set, and a younger, oblique-slip set. We postulate that Jurassic-age dip-slip  
19 faults have been reactivated as strike-slip faults post 5 Ma. Strike-slip motion on NE-SW oriented faults is  
20 consistent with rotation and extrusion of the Kontum and Da Lat blocks. Rotation of the blocks is  
21 consistent with continuum rubble behavior of small crustal blocks under the influence of extrusion-driven  
22 asthenospheric flow.

23

24 Keywords: Vietnam, Indochina, tectonic extrusion, block rotation, strike-slip faults, fault reactivation

25

## 26 **1. Introduction**

27 Onshore Vietnam is a complex region of faulting coupled with a diffuse igneous province that has  
28 been active since the mid-Miocene (Figure 1a, b). However, there is no agreement over the relative ages  
29 of mapped faults and known volcanic centers, as there are several conflicting fault maps and  
30 interpretations of present-day fault activity (e.g. Huchon et al., 1994a; Rangin et al., 1995; Figure 2) for  
31 the southern Vietnamese region. This lack of consensus over relative age becomes problematic when  
32 trying to use structural data to distinguish between the two competing tectonic models for the evolution  
33 of southern Vietnam, that of extrusion tectonics related to the collision of India with Eurasia, which is  
34 thought to have ceased at ~5 Ma (Leloup et al., 2001; Zhu et al., 2009), or that of far-field extension related  
35 to past spreading in the South China Sea region which ceased at ~16 Ma (e.g. Li et al., 2015). Onshore  
36 Vietnam is also characterized by complex stress fields and absolute motions (Michel et al., 2001; Simons  
37 et al., 2007; Tingay et al., 2010; Tran et al., 2013) which cannot easily be explained if the region is a  
38 coherent part of the stable Sundaland block (Tingay et al., 2010).

39 The first model considered here is that of “extrusion” or “escape” tectonics, the process by which  
40 the collision of two tectonic blocks leads to lateral escape of material formerly located between those  
41 blocks. Extrusion has also been invoked to explain the evolution of areas including Alaska and the  
42 Anatolian block in Turkey (Finzel et al., 2011; Gursoy et al., 1997, 2003; Mantovani et al., 2002; Redfield  
43 et al., 2007; Ridgeway and Flesch, 2007; Tapponier et al., 1986). The mechanisms behind extrusion  
44 tectonics remain poorly constrained, however. The proposed extrusion model for Indochina (see e.g.  
45 Chamot-Rooke and Le Pichon, 1999; Chi and Dorobek, 2004; Chi and Geissman, 2013; Flower et al., 1998;

46 Hoang and Flower, 1998; Michel et al., 2001; Morley, 2007; Tingay et al., 2010; Yan et al., 2006) posits  
47 that 1) strong coupling between the asthenosphere and lithosphere and a significant mantle drag torque  
48 has translated the Southern Indochina microplate in response to extrusion of asthenosphere by the  
49 closure of the Tethys Sea and Himalayan collision; and 2) the extruded lithospheric block is characterized  
50 by giant strike-slip faults, smaller scale strike-slip faults and pull-apart basins, and minor normal faulting.

51 Seismic interpretation from two basins offshore from southern Vietnam, however, indicates a  
52 phase of rifting coeval with the propagation of the South China Sea rift zone, and ascribes the presence  
53 of the more recent faulting and onshore diffuse volcanic activity purely to the westward propagation of  
54 this rift and associated thermal subsidence (Fyhn et al., 2009a, b). These data suggest that normal faulting  
55 off-shore predates the voluminous volcanism onshore, and suggests that the volcanic flows erupt into  
56 existing rift or pull-apart basins (Huchon et al., 1994b). However, South China Sea spreading ceased about  
57 16 Ma (Li et al., 2015), and it is unclear whether far-field thermal subsidence can induce fault activity. The  
58 extension-dominated model is expected to produce faults that 1) either pre-date or are synchronous with  
59 volcanic activity, but do not post-date volcanic activity; and 2) have a dominant sense of motion that is  
60 normal.

61 As noted above, existing fault maps are inconclusive (e.g. Huchon et al., 1994a; Rangin et al., 1995;  
62 Figure 2) as to the age relationships between faulting and the basalts of the diffuse igneous province.  
63 These maps are also inconsistent with respect to the sense of motion on the mapped faults (e.g. Searle et  
64 al., 2010; Zhu et al., 2009), making it difficult to reconcile the tectonics of the region with either of the  
65 two models proposed above. The scenario is further complicated by the recognition by local workers (e.g.  
66 Kasatkin et al., 2017) of major strike-slip faults within the Indochina block that dissect southern Vietnam,  
67 forming the Da Lat and associated blocks (Figure 1b), and suspected to be lithospheric in scale. This paper  
68 aims to define the Neogene-Recent tectonic setting and kinematics of the Da Lat block of the onshore  
69 Vietnam region, by analyzing the orientation, kinematics and ages of faults across a sub-region of the

70 block. Fault ages can be constrained by the cross-cutting relationships with dated basalt flows. These  
71 results are used to demonstrate that there has been Cenozoic fault activity in the Da Lat block of southern  
72 Vietnam that (a) post-dates the activity in the diffuse igneous province, (b) potentially reactivates older  
73 faults, (c) is more consistent with an extrusion-based tectonic history than an extension-based tectonic  
74 history for the region, and (d) has implications for how extrusion may be accommodated once a free  
75 surface is no longer present.

76

## 77 **2. GEOLOGIC SETTING**

78 A series of structural, tectonic, and geophysical lines of evidence have been put forward to support  
79 tectonic extrusion as the key driver of tectonic and volcanic activity in Indochina. That evidence includes  
80 the presence of large-scale transform faults such as the Red River Fault Zone (linked to the East Vietnam  
81 Transfer Zone) and the Mae Ping Fault Zone. The pattern of these major strike-slip faults in Southeast Asia  
82 is markedly similar to the pattern of large-scale, left-lateral strike slip faults generated in analog  
83 experiments by Tapponier et al. (1982, 1986). These experiments assume that the western Pacific is acting  
84 as a free surface, that Greater India acts as a rigid indenter, and that Eurasia is segmented and extruded  
85 toward the free surface in order to accommodate the collision. For example, the Red River fault zone  
86 separates the South China block from the Indochina block, and showed left-lateral movement for much  
87 of its history (Rangin et al., 1995). The extrusion model for Indochina further assumes a component of  
88 mantle flow roughly parallel to the strike of the major faults (e.g., Flower et al., 1998; Hoang and Flower,  
89 1998; Yan et al., 2006), which is corroborated by anisotropy recorded in shear-wave splitting data for the  
90 upper mantle beneath the northern part of the Indochina-Shan Tai complex (Bai et al., 2009).  
91 Paleomagnetic and GPS data suggest that the lithosphere is broken into a series of rigid blocks, where the  
92 Kontum and associated blocks may be moving eastwards and rotating, and the Shan Tai block may be

93 rotating and moving to the south (Chamot-Rooke and Le Pichon, 1999; Chi and Dorobek, 2004; Chi and  
94 Geissman, 2013; Michel et al., 2001; Morley, 2007; Tingay et al., 2010). One major challenge to the  
95 extrusion model is that left-lateral motion along the Red River fault zone, a key signature of extrusion of  
96 Indochina, ceased around 17 Ma, and became right-lateral motion by 5.5 Ma (e.g., Leloup et al., 2001; Zhu  
97 et al., 2009). This cessation of left-lateral movement is frequently considered to mark the end of extrusion  
98 of the Indochina block, but may instead mark a change in regional or local kinematics. Coeval with the  
99 change in motion is inversion of some of the northern-most basins along the Red River Fault Zone, such  
100 as the Song Hong Basin (Fyhn et al., 2018). Inversion can also be noted in Cuu Long and Nam Con Son  
101 basins of south Vietnam (Pubellier & Morley, 2014). The cause of this change in plate kinematics is  
102 variously ascribed to the ridge jump in the SCS, a change in Indian indenter motion (e.g. coupling the  
103 Indian and Burmese blocks; Fyhn et al., 2009a, b), or an additional plate tectonic reconfiguration in the  
104 region such as the collision of Australian fragments to the SE of Sundaland (Pubellier & Morley, 2014).

105        Extensional tectonics in Indochina have been well documented, starting with Jurassic-Cretaceous age  
106 back-arc rifting, due to the subduction of the proto-Pacific crust under Vietnam, Borneo and South China  
107 (Nam, 1995; Morley, 2012). Jurassic-Cretaceous rift locations were partially influenced by weak zones  
108 resulting from the Indosinian Orogeny, the collision of the Sibumasu, South China and Indochina blocks  
109 during the Triassic (Lepvrier et al., 2004; Pubellier & Morley, 2014). The Jurassic-Cretaceous event was  
110 initially followed by Late Cretaceous rifting along the proto-South China basin (Barckhausen et al., 2014;  
111 Chung et al., 1997; Zhou et al., 1995) and subsequently by the opening of the SCS, which experienced  
112 ocean spreading from 32 Ma. Spreading either ceased at 20.5 Ma (Barckhausen et al., 2014) or at 16 Ma  
113 for the southwest sub-basin of the SCS, closest to our study area (Li et al., 2015). After SCS spreading  
114 ceased, rifting may have propagated onshore, while lingering upper mantle upwelling generated ongoing  
115 diffuse seamount activity within the SCS (Barckhausen et al., 2014; Cullen et al., 2010; Matthews et al.,  
116 1997; Swiecicki & Maynard, 2009; Yan et al., 2006). The date of 16 Ma also corresponds with the change

117 in motion along the Red River fault zone described above, marking a change in regional plate kinematics.  
118 Regional compression and uplift led to widespread erosion across southern Indochina during the  
119 Paleocene, with the development of significant unconformities across southern Indochina (Fyhn et al.,  
120 2009a; Tri et al., 2011).

121 After the cessation of SCS rifting, regional uplift rates also became more rapid, contemporaneous  
122 with the initiation of onshore volcanism in the Miocene (Carter et al., 2000; Fyhn et al., 2009a; Wang et  
123 al., 2006). Onshore, eruptions of basalt have occurred in four significant phases since the Miocene: 17-12  
124 Ma, 9-7.4 Ma, 5.4-1.75 Ma and 0.7-0.57 Ma (Tri et al., 2011). Fyhn et al. (2009a, b), Cullen et al. (2010)  
125 and Savva et al. (2013) asserted that the observed patterns of uplift and on- and offshore volcanism are  
126 purely the product of regionally propagating extension following the cessation of oceanic rifting, though  
127 they do not otherwise explicitly account for the large volume of onshore volcanics. All sets of work  
128 produced seismic lines across the offshore Phu Khanh, Cuu Long, and Nam Con Song basins and interpret  
129 two to three stages of rifting, separated by a period of tectonic quiescence. Crucially, the last rifting phase  
130 is after the cessation of active SCS spreading (Matthews et al., 1997; Swiecicki & Maynard, 2009; Savva et  
131 al., 2013). In the Phu Khanh basin, rifting is interpreted to be transtensional and related to the offshore  
132 trace of the Red River Fault Zone (Fyhn et al., 2009a, b; Cullen et al., 2010; Savva et al., 2013). Rifting in  
133 the Cuu Long and Nam Con Song basins is interpreted by these authors to be related to continued regional  
134 extension associated with SCS extension, even though active spreading to the east has ceased (Matthews  
135 et al, 1997; Fyhn et al., 2009a, b; Dung et al., 2018). Volcanic eruptions there appear to have been  
136 emplaced along fault planes, suggesting rifting predates volcanic activity (Fyhn et al., 2009 a, b), but it is  
137 not clear if this pattern continues onshore, where the major tectonic regime during the Pliocene-Holocene  
138 is thought to be thermal subsidence (Tri et al., 2011).

139 There are thus a number of observations that are not well explained by an extensional tectonic model  
140 for southern Vietnam, such as the ongoing and voluminous volcanism, the origins of offshore rifting after

141 SCS spreading ended, and the change in fault motion of the Red River fault. Using fault geometries and  
142 timing, palinspastic reconstructions, and geophysical data, some workers have thus instead attempted to  
143 reconcile the extrusion model of Indochina with the opening of the SCS. The end-member models state  
144 that SCS rifting is completely independent of the extrusion of Indochina (e.g., Chung et al., 1997; Clift et  
145 al., 2008; Yan et al., 2006), or that the opening of the SCS basin is a direct consequence of the stress regime  
146 imposed by the extrusion of Indochina (e.g., Briaies et al., 1993). Zhou et al. (1995) and Fyhn et al. (2009a)  
147 propose that extrusion tectonics had some effect on ridge axial relocations in the SCS as noted by Briaies  
148 et al. (1993), but that initial opening of the basin was independent of the India-Himalaya collision. Cullen  
149 et al. (2010) propose that neither slab rollback in the western Pacific, nor extrusion of Indochina can fully  
150 explain the tectonic setting of southern Vietnam, and invoke additional asthenospheric upwelling to  
151 provide sufficient crustal extension, heat flow, and volcanism. Seismic data support the presence of a  
152 shallow mantle thermal anomaly underlying Indochina, which may reflect diffuse mantle upwelling in  
153 support of dispersed volcanic activity (Liu et al., 2004), and the region has documented high heat flow  
154 (Duchkov et al., 1992; Uyeda, 1994).

155 Further, GPS data, albeit a sparse dataset, indicates that the Sunda block moves as a rigid and  
156 coherent unit, with an absolute motion to the ESE (Michel et al., 2001; Simons et al., 2007; Tran et al.,  
157 2013). However, the stress field across the Sunda block is heterogeneous, rather than subparallel to the  
158 absolute motion vector (Tingay et al., 2010; Van Nquyen & Hoai, 2019) suggesting that the question of  
159 whether this region can best be described in terms of block tectonics or continuous deformation (Calais  
160 et al., 2006) is unresolved. In the case of Indochina, the block tectonics hypothesis of Calais et al. (2006)  
161 is potentially compatible with an extrusion-driven origin for Neogene-Recent deformation in the region,  
162 whereas the continuous deformation field hypothesis is more compatible with regional stretching and  
163 thermal subsidence related to South China Sea rifting.

164 Existing data shows other discrepancies in the Da Lat and surrounding blocks (Figure 1b, 2), where  
165 previously generated remote sensing and field focused maps (e.g. Huchon et al., 1994a; Rangin et al.,  
166 1995) do not agree on fault locations or trajectories, nor on whether faults cut the voluminous basalt  
167 flows or whether the flows overrun the major faults. Van Nguyen & Hoai (2019) provide several data  
168 points where faults are observed to cut the Neogene or Quaternary basalts, although the bulk of their  
169 data points are in the Cretaceous age granites. Studies of basalt flow ages (e.g. An et al. 2017; Lee et al.  
170 1998) show that many of the flows in the Da Lat block are significantly younger than 5 Ma, indicating that  
171 volcanism and potentially faulting are ongoing in the study area.

172

### 173 **3. METHODS**

174 This study was a joint remote-sensing and field study. We interpreted lineaments across the field  
175 area, using both Landsat ETM+ data and SPOT data. Figure 3 shows Landsat ETM+ and SPOT coverages,  
176 together with field locations. Landsat ETM+ datasets were sourced from the Global Land Cover Facility  
177 (GLCF) and the SPOT data were sourced from Apollo Mapping. Landsat ETM+ data were downloaded as  
178 separate bands and combined into a false color composite. Bands 531 were combined as RGB in ArcGIS.  
179 This raster was stretched using the histogram equalize operation. Landsat ETM+ data were also combined  
180 as a true color composite using bands 321 as RGB in ArcGIS. This imagery was blended using a standard  
181 deviation stretch. SPOT data was provided as a true color composite by the vendor. The data were already  
182 georeferenced to the Landsat ETM+ reference frame. Digital Elevation Model (DEM) data were also  
183 sourced from the GLCF and displayed as classified datasets in ArcGIS. As for the Landsat ETM+ datasets,  
184 the interactive map tool was used to define the study area and locate the datasets. The remote datasets  
185 were compiled into an ArcGIS project and the field locations and other information were added by  
186 database upload or by georeferencing jpg files. Other information comprises: 1) maps from Huchon et al.



187 (1994a), Rangin et al. (1995), and the Department of Geology and Minerals, Vietnam; and 2) locations  
188 with dated basalt samples from Lee et al. (1998) and An et al. (2017).

189 Lineaments were picked from the satellite maps on the basis of textural changes in the images, or by  
190 considering the changes in stream patterns. For example, abrupt changes in direction of stream channels,  
191 or abnormally straight segments of streams, indicate the presence of joints or faults in the subsurface  
192 governing that stream pattern (Drury, 2004). In addition, linear changes in texture of the land surface  
193 often indicate a fault-controlled change, although care must be taken to avoid regions where the land  
194 surface has been altered by humans. Such regions can be identified by the typical regular checkerboard  
195 pattern of cultivated fields and field boundaries and the proximity to dwellings. It should be noted that  
196 there are two resolutions of data in the imagery and thus there will be areas where lineaments may be  
197 more densely picked than others; in addition, there are regions of the study area that are densely  
198 populated and cultivated, such that there is not an even coverage of lineaments across the study area.  
199 Once picked, the lineament map was classified using the ArcGIS Grouping Analysis algorithm, nearest  
200 neighbor option, within ArcGIS. The lineaments were classified into 50, 75 and 100 bins, and the 75-bin  
201 option was used to compare the lineaments to the field dataset and known earthquake locations in order  
202 to produce a predicted deep-seated fault map of the area. The predicted deep-seated faults were picked  
203 based on dominant orientation within the lineament clusters. The 75-bin option was used because, on  
204 inspection, this option did not split trends that were apparent from the satellite data, which the 100-bin  
205 option was prone to doing. The 50-bin option gave clusters that were too coarse when compared to the  
206 field dataset.

207 We also undertook a reconnaissance field trip in 2016 to the southern part of the Central  
208 Highlands, near Ho Chi Minh City, Buon Ma Thuot, and Vung Tau. We observed lithology at every stop,  
209 and where relevant, we took measurements of bedding attitude, fault attitude and fault lineation pitch  
210 within the fault plane. At each site, we noted the relationship of faults and the host lithology, considering

211 whether the fault terminated against lithological elements, or cut all observable lithologies. On our return  
212 to the lab, these data were synthesized using GIS and Stereonet 10™ to determine similarity in fault  
213 orientations, possible fault kinematics and the relationship to the lineament map.

214 To clarify the age of structural elements, the age of one alkali basalt flow (field sample number  
215 2016-CH-10, retrieved from location 10.5076°N, 107.2729°E, and 229 ft. elevation), was determined using  
216 <sup>40</sup>Ar/<sup>39</sup>Ar methods at the Oregon State University Argon Geochronology Lab in Corvallis, Oregon. The  
217 sample was crushed, sieved to ~300 μm grain size, rinsed in distilled water and dried at low temperature  
218 in an oven (~80°C), then mildly leached to remove impurities. The procedure for leaching was a 20 min.  
219 soak in 5% HNO<sub>3</sub> in an ultrasonic bath, followed by 3 rinses in distilled water, then a 20 min. soak in distilled  
220 water in the ultrasonic bath and 3 more distilled water rinses; the sample was then again dried at 80°C or  
221 lower in the oven. Following this preparation procedure, the sample was irradiated in the TRIGA  
222 experimental reactor at the OSU Radiation Center at 1 MW power. The neutron flux during irradiation  
223 was monitored using the FCT-NM standard, with an adopted age of 28.20 ± 0.02 Ma (after Kuiper et al.,  
224 2008), and a <sup>40</sup>Ar/<sup>39</sup>Ar = 9.733 ± 0.008 and J-value of 0.001615 ± 0.000001. For mass spectrometry, the  
225 sample was analyzed by incremental heating using a bulk CO<sub>2</sub> laser heating method on the ARGUS-VI-D  
226 instrument at OSU. Ages were determined using a decay constant of 5.53 ± 0.05 × 10<sup>-10</sup> a<sup>-1</sup> (Steiger and  
227 Jäger, 1977) using age correction methods after Min et al. (2000). Heating plateau ages were determined  
228 using an error weighted mean of plateau steps. Additional standard and procedural blank results are  
229 available in the Supplementary Information.

230

## 231 **4. RESULTS**

### 232 **4.1 Remote sensing**

233 Figure S1 shows lineament orientations mapped via remote sensing across the study area. In total,  
234 2323 lineaments were picked across the study area using the methods described above. Figure S2 shows  
235 a rose diagram of those lineament orientations, and shows a strong N-S to NE-SW fault trend, with very  
236 minor components in other cardinal directions. 11.7% of the data is distributed between a bearing of 031  
237 and 040. Figure 4 shows the classified lineaments, which were classified using the ArcGIS algorithm as  
238 described above, and each cluster is shown in a different color. Note that there is a strong preferred  
239 orientation within many of these clusters. For example, in the NW of the study area and to the W of the  
240 lake, there is a teal-colored cluster which trends NNE-SSW. These lineaments all cut basalt flows which  
241 have been previously dated as 4.3 +/- 0.2 Ma (An et al. 2017) or ranging between 2.42 +/- 0.08 Ma (south  
242 of Xuan Loc center) to 0.24 +/- 0.06 Ma (north of Xuan Loc center; Lee et al., 1998; Figure 5) and thus fall  
243 within the second youngest and youngest phases of basalt extrusion. Figure 5 further shows that the  
244 lineaments do not preferentially cut basalts or clastic units, but are distributed between the Jurassic to  
245 Quaternary formations without an apparent skew to one type of formation.

246 These data imply that there is a strong lineament orientation trending NE-SW across the study  
247 area and that is in many cases younger than 4.3 +/- 0.2 Ma (An et al. 2017). Below we compare the  
248 lineament data with the field data to further assess the nature of these lineaments.

249

## 250 **4.2 Field data**

251 Here we describe field observations for a series of sites across the study area (Table 1, Figure 3),  
252 in order of observation. All strike and dip data is expressed using the Right Hand Rule convention, so no  
253 dip quadrant is listed.

254 At location 1 (Figure 3), a series of faults cutting Jurassic sediments were observed (Figure 6). One  
255 key fault (Figure 6a, b) had an attitude of 024/88 with two sets of lineations, one pitching 16°SW and the

256 other pitching 80°SW (Figure 6c). Figure 8b shows that the sub-horizontal lineation cross-cuts the dip-slip  
257 lineation on this fault surface. On the other side of the same quarry, faults were observed with attitudes  
258 of 027/58 (dip-slip lineations) and 015/48 (no visible lineations) (Figure 6c). We could not identify whether  
259 the oblique slip lineaments were left-lateral or right-lateral as there were no identifiable “steps” in these  
260 lineaments.

261 At location 2 (Figure 3), a series of faults cutting the Soc Lu Formation were observed (e.g. Figure  
262 7a). The Soc Lu Formation at this locality has been dated to 4.3 +/- 0.2 Ma (An et al., 2017). Field  
263 observations of plagioclase and biotite phenocrysts in Soc Lu volcanics suggest that the Soc Lu Formation  
264 eruptives include basaltic andesite, and the observed flow coverage (not shown in Figure 5 due to its  
265 limited extent) suggests a relatively small flow unit within the Xuan Loc volcanic center. The faults at this  
266 location strike NE-SW and are sub-vertical. One fault has an attitude of 036/76 and two other fault  
267 surfaces are oriented 023/85 and 028/80. On each fault surface, sub-horizontal lineations were observed,  
268 with pitches of 12°NE, 12°NE and 18°NE respectively (Figure 7b). Again, we were not able to discern  
269 whether the lineations gave a sense of left- or right-lateral movement because convincing “steps” in the  
270 lineations were not identifiable on these fault planes.

271 At location 3 (Figure 3), an old quarry in the alkali basalts of the Xuan Loc Formation where mantle  
272 xenoliths were observed, additional faults were observed with orientations of 172/57 and 121/80. The  
273 first of these faults was marked by heavily foliated basalt, and neither fault displayed lineations.

274 Locations 4-7 are clustered close together in faulted Cretaceous age granites near Vung Tau. These  
275 granites are part of the Deo Ca complex which has been dated at either 88-92 Ma or c. 118 Ma by U-Pb  
276 zircon geochronology (Ngyuen et al. 2004; Shellnutt et al., 2013; Hennig et al., 2018). One major fault with  
277 several strands and a damage zone of tens of cm wide has an attitude of 236/84 (Figure S3a). Other fault  
278 surfaces have attitudes of 228/74 and 294/76, and these fault zones contain black material that may be

279 pseudo-tachylite or later intruded and sheared mafic material (Figure S3b). The major fault zone oriented  
280 at 236/84 corresponds to the known Ca Na-Vung Tau fault zone (Figure 1b) which bounds the Da Lat block  
281 to the south.

282 At location 8, an alkali basalt quarry north of Vung Tau, a series of joints were measured, as there  
283 was no visible evidence of faulting on the safely accessible exposed faces of this active quarry. The pole  
284 figure for this dataset is found in Figure S4. A strong cluster of poles is found marking a joint set oriented  
285 ENE-WSW, amongst a near uniform distribution of other joints. We infer that this outcrop was cut by a  
286 combination of columnar, i.e. basaltic cooling joints, and a systematic set of joints oriented ENE-WSW.

287 Sample 2016-CH-10 from location 8 was determined using  $^{40}\text{Ar}/^{39}\text{Ar}$  age dating methods to have  
288 an initial eruption age of  $0.600 \pm 0.004$  Ma ( $2\sigma$ ). This weighted mean plateau age is consistent with ages  
289 calculated using the alternative total fusion ( $0.599 \pm 4$  Ma), normal isochron ( $0.599 \pm 0.006$  Ma), and  
290 inverse isochron methods ( $0.599 \pm 0.006$  Ma) (see Supplementary Information for additional raw data and  
291 plateau age results for this analysis). The mean squared weighted deviation for the plateau age is 0.002  
292 Ma, and calculated K/Ca ratio is  $0.21 \pm 0.09$  ( $2\sigma$ ).

293 These data indicate that there are small-scale faults and fractures that both pre and post-date the  
294 basalt flows across the studied area of the Da Lat block. The following section will compare this dataset  
295 to the lineament dataset and derive a model for the generation of the small-scale faults and fractures.

### 296 **4.3 Combining the datasets**

297 The small-scale faults and fractures of the field dataset are overall interpreted to be the classified  
298 lineaments of the remote sensing dataset. However, some of the faults in the field dataset predate the  
299 basalts while others post-date the basalts. In addition, at Location 1, the fault in the Jurassic-Cretaceous  
300 sediments has been reactivated, indicating the occurrence of multiple events. We infer that the faults  
301 documented at Locations 1 and 4-7 with age constraints of either post-Jurassic or post-Cretaceous (that

302 is, post c. 118 Ma or post 88-92 Ma) are deeper seated or pre-existing faults. These pre-existing faults  
303 predate Late Cretaceous and younger sedimentation and basalt effusion in the region. Such faults can be  
304 estimated from the average orientations of classified lineament clusters as shown in Figure 8. In some  
305 cases, additional data such as earthquake event locations were used to identify these deeper seated or  
306 pre-existing faults. We infer that many of these deeper and/or pre-existing faults initiated as rifts in the  
307 Jurassic or Cretaceous and have since been reactivated as strike-slip faults during later deformation. In  
308 some cases (e.g., Figure 9a, b) classic lineament patterns are observed that suggest reactivation of the  
309 deeper-seated fault as a transpressional flower structure.

#### 310 **4.4 Model for faulting across the Da Lat Block**

311         Considering the faults at locations 1 and 2, we infer that the NE-SW trending faults cutting the  
312 basalt flows are genetically related to the NE-SW trending faults in the Jurassic sediments. We postulate  
313 that (a) the Jurassic-Cretaceous, steeply dipping dip-slip faults or joints have been reactivated as strike-  
314 slip faults during the Neogene (location 1), and (b) this reactivation of deeper-seated faults led to the  
315 generation of damage in the overlying Neogene basalts. This damage is manifested as the smaller-scale  
316 strike slip faults observed at location 2 and potentially as the fractures noted and measured at location 8,  
317 although we acknowledge that these fractures may be due to a different phase of relatively recent  
318 deformation within the Da Lat block. The development of strike-slip motion on faults oriented dominantly  
319 NE-SW within the Da Lat block is consistent with the continued extrusion of this block within the large-  
320 scale shear zone created by the Three Pagodas Fault and Ailo Shan-Red River-East Vietnam shear zones  
321 (Figure 1a). We therefore propose that extrusion did not cease at 5 Ma as has been previously suggested,  
322 but is ongoing, and is now accommodated by the rotation of blocks such as Da Lat and by internal  
323 deformation within this part of Sundaland. We speculate that the kinematics of the extrusion regime  
324 changed with the change in regional plate dynamics, as discussed in Section 2, and with the effective  
325 removal of the Western Pacific free surface by the collision of Luconia, Dangerous Grounds and Reed Bank

326 with NW Borneo and Palawan (Hall, 2002; Hall et al., 2008; Clift et al., 2008). In our conceptual model, the  
327 individual blocks shown in Figure 1b are moving semi-independently, similar to the continuum  
328 deformation style proposed by Calais et al. (2006). Under the existing extrusion model, Vietnam and the  
329 Da Lat block move to the SE (e.g. Tingay et al., 2010). Under our new model, the Da Lat block moves semi-  
330 independently to the SW to accommodate extrusion.

331

## 332 **5. DISCUSSION**

333 Contrary to existing literature (e.g. Rangin et al., 1995; Searle et al., 2010; Zhu et al., 2009) which  
334 states that faulting of both extrusion and extension regimes has ceased in the Indochina Peninsula, our  
335 results demonstrate that faulting has been more recent than  $4.3 \pm 0.2$  Ma (An et al. 2017),  $0.600 \pm 0.004$   
336 (this study), or  $0.24 \pm 0.1$  Ma (Lee et al., 1998). This is more recent than the postulated end of extrusion  
337 based on the change in motion of the Red River Fault Zone (5.5 Ma; Leloup et al., 2001; Zhu et al., 2009)  
338 and, significantly, the cessation of rifting in the South China Sea (16 Ma: Li et al, 2015). Thus, a tectonic  
339 regime more complex than thermal subsidence must be operating across onshore Vietnam, and we  
340 propose that this regime is extrusion-related. We do not favor the extension argument because the key  
341 faults observed at locations 1 and 2 were oriented NE-SW and showed oblique to strike-slip movement,  
342 whereas under an extensional regime, faults in this orientation would show oblique to dip-slip movement.  
343 Our proposed model of continuum block deformation of the onshore Vietnam region and southwestwards  
344 movement of the Da Lat block further predicts dominantly left-lateral movement on the NE-SW oriented  
345 strike-slip faults that were observed in the field and on the East Vietnam Transfer Zone (Trinh et al., 2015).  
346 While the lineations observed to-date do not show stepwise patterns that allow us to identify the sense  
347 of motion to test this prediction, because we do not observe dip-slip motion on these faults we can still  
348 effectively rule out an extension-dominated regime related to the SCS. The presence of strike-slip faulting

349 is compatible with the results from extensive field mapping in the Cretaceous granites reported by Van  
350 Nguyen and Hoai (2019). Van Nguyen and Hoai (2019) further reported four stress regimes operating  
351 since the end of the Oligocene and interpreted a rotation in the stress field associated with extrusion. We  
352 note that there is some spatial variation in each stress field across the Song Ba fault, which separates the  
353 Kontum and Da Lat blocks. Thus, we surmise that the Van Nguyen and Hoai (2019) dataset is compatible  
354 with our model.

355 We have generated a proposed pre-Neogene fault map (Figure 8) for a sub-region of the Da Lat  
356 block, based upon lineament mapping and cluster analysis, which is distinctly different from the fault  
357 maps generated by previous authors and shown in Figure 2. Our fault map has a denser distribution of  
358 structural features than the maps shown in Figure S5 and consists of shorter discrete fault segments, due  
359 to improved imagery resolution. Our fault map is also unique in that it constrains the ages of the remotely  
360 sensed faults (post-Jurassic and pre-Neogene, i.e. pre-basalt effusion) and distinguishes these older,  
361 deeper-seated faults from the more recent, smaller-scale faults and fractures visible on the lineament  
362 map that cut Neogene-Recent basalt flows. We further suggest that the older structures (Figure 8) date  
363 from late Jurassic subduction under the leading edge of the Kontum block and contemporaneous,  
364 associated intraplate extension, as documented by Tri and Bao (2011). An episode of basin inversion may  
365 have reactivated these faults in the late Miocene-early Pliocene (Tri and Bao, 2011) due to a change in  
366 direction of Indian plate subduction, coincident with the change in sense of motion of the Red River Fault  
367 Zone (e.g., Leloup et al., 2001; Zhu et al., 2009).

368 The Red River Fault Zone ceased left lateral motion around 17 Ma and initiated right-lateral  
369 motion approximately 5.5 Ma (e.g., Leloup et al., 2001; Zhu et al., 2009; Zuchiewicz et al., 2013). As noted  
370 above, this change was previously inferred to mark the end of extrusion of Indochina, but instead we  
371 suggest that this marks a change in the kinematics of the extrusion process. During right-lateral motion,  
372 the major block being extruded is the South China block (Guo et al., 2001; Meng et al., 2005). However,



373 this does not account for asthenospheric flow associated with the extrusion of Indochina, or for  
374 documented ongoing volcanism (e.g., the 1923 eruption of Ile des Cendres), which suggests continued  
375 mantle flow and upwelling (e.g. Hoang and Flower, 1998). To accommodate the motion of the mantle  
376 conveyor belt beneath, the Shan Tai, Kontum, Da Lat and other blocks would need to rotate within the  
377 confines of the larger scale shear zone defined by the Red-River – East Vietnam Transform and the Mae  
378 Ping Fault Zones. This is required because there is no free surface into which these blocks can be extruded,  
379 given their position in the core region of Sundaland. This suggestion posits a strong coupling between the  
380 asthenosphere and the lithospheric blocks in this area, in contrast to the relatively weak mantle drag  
381 torque inferred for areas with high subduction zone torques (e.g., the Nazca and Pacific plates; Chapple  
382 & Tullis, 1977). We therefore suggest that extrusion tectonics require a strong lithosphere-asthenosphere  
383 coupling, and that once the free surface is removed by other tectonic processes, block rotation is the  
384 inevitable consequence of ongoing mantle flow.

385         Paleomagnetic and GPS data from the core of Sundaland show that the Kontum block region is  
386 likely moving to the east and rotating clockwise within Sundaland (Chamot-Rooke and Le Pichon, 1999;  
387 Chi and Dorobek, 2004; Chi and Geissman, 2013; Cung and Geissman, 2013; Michel et al., 2001; Morley,  
388 2007; Tingay et al., 2010; Tran et al., 2013). This rotation is consistent with a regional model whereby  
389 Sundaland is composed of not a rigid core, but instead a continuum rubble of fragments that interact and  
390 “jostle” or rotate with respect to one another under regional stresses. The eastward motion of the  
391 Kontum block is consistent with a continued overall extrusion of material from the Himalayan collision to  
392 the east and southeast. The Da Lat block lacks GPS and paleomagnetic data at a fine enough scale to  
393 resolve the proposed southwest-wards motion and merits further investigation (Van Nguyen and Hoai,  
394 2019 and references therein).

395

396 **6. CONCLUSIONS**

397 Results from remote sensing show a strong NE-SW fault trend for southern Vietnam, with additional,  
398 minor N-S, E-W and NW-SE trends. The dominant trend characterized as NE-SW is composed of a dataset  
399 dispersed between N and NE orientations, with a peak at the NNE orientation. Many of these lineaments  
400 cut basalt flows previously dated at  $4.3 \pm 0.2$  Ma (An et al. 2017) or  $0.24 \pm 0.1$  Ma (Lee et al., 1998), as  
401 well as one measured here to be  $0.600 \pm 0.004$  Ma. Fault orientations observed in the field fall into this  
402 NE-SW trending class, and are sub-vertical. In the basalt flows (with eruption ages  $< 5$  Ma) these faults  
403 have oblique lineations with a strong strike-slip component. In the Jurassic sediments, these faults show  
404 two sets of lineations; an older, dip-slip set, and a younger, oblique-slip set.

405 These results indicate that the NE-SW dominant set of faults cuts basalt flows significantly younger than  
406 5 Ma, and movement on these faults is therefore younger than both the cessation of rifting in the SCS and  
407 the cessation of sinistral movement on the Red River Fault. We infer that the NE-SW trending faults cutting  
408 the basalt flows are related to the NE-SW trending faults in the Jurassic sediments, and postulate that  
409 Jurassic-age dip-slip faults have been reactivated as strike-slip faults post 5 Ma. Strike-slip motion on NE-  
410 SW oriented faults is consistent with rotation and extrusion of the Kontum and Da Lat blocks, rather than  
411 extension and subsidence, in which case dip-slip (normal) motion would be expected. Furthermore,  
412 rotation of the blocks is consistent with continuum rubble behavior of small crustal blocks under the  
413 influence of extrusion-driven asthenospheric flow.

414

415 **7. Acknowledgments.** CMB and LJE acknowledge a University of Nebraska-Lincoln College of Arts and  
416 Sciences International Partnerships Grant and NSF Grant EAR-1758972. We also acknowledge the OSU  
417 Argon Geochronology Lab, particularly Dan Miggins, who made the measurements on the sample

418 referenced in this paper. Remote sensing data was purchased from Apollo Mapping. Figure 5 was created  
419 using this data and VAST maps by Nathan Sorsen as part of an undergraduate research project.

420

## 421 **8. REFERENCES**

422 An, A-R., Choi, S.H., Yu, Y., and Le, D-C., 2017. Petrogenesis of Late Cenozoic basaltic rocks from southern  
423 Vietnam. *Lithos*, v. 272-273, p. 192-204.

424 Bai, L., Iidaka, T., Kawakatsu, H., Morita, Y., and Dzung, N. Q., 2009, Upper mantle anisotropy beneath  
425 Indochina block and adjacent regions from shear-wave splitting analysis of Vietnam broadband  
426 seismograph array data: *Physics of the Earth and Planetary Interiors*, v. 176, p. 33-43.

427 Barckhausen, U., Engels, M., Franke, D., Ladage, S., and Pubellier, M., 2014, Evolution of the South China  
428 Sea: Revised ages for breakup and seafloor spreading: *Marine and Petroleum Geology*, v. 58, p. 599-611.

429 Briaux, A., Patriat, P., and Tapponier, P., 1993, Updated interpretation of magnetic anomalies and seafloor  
430 spreading stages in the South China Sea: Implications for the Tertiary tectonics of SE Asia: *Journal of*  
431 *Geophysical Research*, v. 98, p. 6299-6328.

432 Calais, E., Dong, L., Wang, M., Shen, Z., & Vergnolle, M. (2006). Continental deformation in Asia from a  
433 combined GPS solution. *Geophysical Research Letters*, 33(24).

434 Carter, A., Roques, D., and Bristow, C. S., 2000, Denudation history of onshore Central Vietnam:  
435 constraints on the Cenozoic evolution of the western margin of the South China Sea: *Tectonophysics*, v.  
436 322, p. 265-277.

437 Chamot-Rooke, N., and Le Pichon, X., 1999, GPS determined eastward Sundaland motion with respect to  
438 Eurasia confirmed by earthquake slip vectors at Sunda and Philippine trenches: *Earth and Planetary*  
439 *Science Letters*, v. 173, p. 439-455.

440 Chapple, W. M., & Tullis, T. E. (1977). Evaluation of the forces that drive the plates. *Journal of geophysical*  
441 *research*, 82(14), 1967-1984.

442 Chi, C. T., and Dorobek, S. L., 2004, Cretaceous palaeomagnetism of Indochina and surrounding regions:  
443 Cenozoic tectonic implications, in Malpas, J., Fletcher, C. J. N., Ali, J. R., and Aitchison, J. C., eds., *Aspects*  
444 *of the Tectonic Evolution of China*, Volume 226: London, Geological Society of London, p. 273-287.

445 Chi, C. T., and Geissman, J., 2013, A review of the paleomagnetic results of Cretaceous rock formations  
446 from Vietnam, Indochina and South China, their Cenozoic tectonic implications: *Journal of Geodynamics*,  
447 v. 69, p. 54-64.

448 Chung, S.-L., Cheng, H., Jahn, B., O-Reilly, S. Y., and Zhu, B., 1997, Major and trace element, and Sr-Nd  
449 isotope constraints on the origin of Paleogene volcanism in South China prior to the South China Sea  
450 opening: *Lithos*, v. 40, p. 203-220.

451 Clift, P., Lee, G. H., Duc, N. A., Barckhausen, U., Van Long, H., and Zhen, S., 2008, Seismic reflection  
452 evidence for a Dangerous Grounds miniplate: No extrusion origin for the South China Sea: *Tectonophysics*,  
453 v. 27, doi: 10.1079/2007TC002216.

454 Cullen, A., Reemst, P., Henstra, G., Gozzard, S., and Ray, A., 2010, Rifting of the South China Sea: New  
455 perspectives: *Petroleum Geoscience*, v. 16, p. 273-282.

456 Cung, T.C. & Geissman, J. W. (2013). A review of the paleomagnetic data from Cretaceous to lower Tertiary  
457 rocks from Vietnam, Indochina and South China, and their implications for Cenozoic tectonism in Vietnam  
458 and adjacent areas. *Journal of Geodynamics*, 69, 54-64.

459 Drury, S.A., 2004. Image interpretation in Geology (3<sup>rd</sup> Ed). Routledge, 304 pp.

460 Duchkov, A. D., Yem, N. T., Toan, D. V., and Bak, C. V., 1992, First estimates of heat flow in Vietnam: Sov.  
461 Geol. Geophys., v. 33, p. 92-96.

462 Dung, B. V., Tuan, H. A., Van Kieu, N., Man, H. Q., Thuy, N. T. T., & Huyen, P. T. D. (2018). Depositional  
463 environment and reservoir quality of Miocene sediments in the central part of the Nam Con Son Basin,  
464 southern Vietnam shelf. *Marine and Petroleum Geology*, 97, 672-689.

465 Finzel, E. S., Flesch, L. M., and Ridgeway, K. D., 2011, Kinematics of a diffuse North American-Pacific-Bering  
466 plate boundary in Alaska and western Canada: *Geology*, v. 39, p. 835-838.

467 Flower, M. F. J., Tamaki, K., and Hoang, N., 1998, Mantle extrusion: A model for dispersed volcanism and  
468 DUPAL-like asthenosphere in East Asia and the Western Pacific, in Flower, M. F. J., Chung, S.-L., Lo, C.-H.,  
469 and Lee, T.-Y., eds., *Mantle Dynamics and Plate Interactions in East Asia*, Volume 27, American  
470 Geophysical Union, p. 67-88.

471 Fyhn, M. B. W., Boldreel, L. O., and Nielsen, L. H., 2009a, Geological development of the Central and South  
472 Vietnamese margin: Implication for the establishment of the South China Sea, Indochinese escape  
473 tectonics, and Cenozoic volcanism: *Tectonophysics*, v. 478, p. 184-214.

474 Fyhn, M. B. W., Nielsen, L. H., Boldreel, L. O., Thang, L. D., Bojesen-Koefoed, J., Petersen, H. I., Huyen, N.  
475 T., Duc, N. A., Dau, N. T., Mathiesen, A., Reid, I., Huong, D. T., Tuan, H. A., Hien, L. V., Nytoft, H. P., and  
476 Abatzis, I., 2009b, Geological evolution, regional perspectives and hydrocarbon potential of the northwest  
477 Phu Khanh Basin, offshore Central Vietnam: *Marine and Petroleum Geology*, v. 26, p. 1-24.

478 Fyhn, M. B., Cuong, T. D., Hoang, B. H., Hovikoski, J., Olivarius, M., Tuan, N. Q., Tung, N.T., Huyen, N.T.,  
479 Cuong, T.X., Nytoft, H.P & Abatzis, I. (2018). Linking Paleogene Rifting and Inversion in the Northern Song

480 Hong and Beibuwan Basins, Vietnam, With Left-Lateral Motion on the Ailao Shan-Red River Shear Zone.  
481 *Tectonics*, 37(8), 2559-2585.

482 Guo, L., Zhong, Z., Wang, L., Shi, Y. S., Li, H., & Liu, S. W. (2001). Regional tectonic evolution around  
483 Yinggehai basin of South China Sea. *Geological Journal of China Universities*, 7(1), 1-12.

484 Gursoy, H., Piper, J. D. A., and Tatar, O., 2003, Neotectonic deformation in the western sector of tectonic  
485 escape in Anatolia: paleomagnetic study of the Afyon region, central Turkey: *Tectonophysics*, v. 374, p.  
486 57-79.

487 Gursoy, H., Piper, J. D. A., Tatar, O., and Temiz, H., 1997, A palaeomagnetic study of the Sivas Basin, central  
488 Turkey: Crustal deformation during lateral extrusion of the Anatolian Block: *Tectonophysics*, v. 271, no.  
489 89-105.

490 Hall, R., 2002. Cenozoic geological and plate tectonic evolution of SE Asia and the SW Pacific: computer-  
491 based reconstructions, model and animations. *Journal of Asian Earth Sciences*, v. 20 (4) p353-431.

492 Hall, R., van Hattum, M., Spakman, W., 2008. Impact of India–Asia collision on SE Asia: the record in  
493 Borneo. *Tectonophysics*, 451 pp. 366-369.

494 Hennig, J., Breitfeld, H. T., Gough, A., Hall, R., Long, T. V., Kim, V. M., & Quang, S. D. (2018). U-Pb zircon  
495 ages and provenance of upper Cenozoic sediments from the Da Lat Zone, SE Vietnam: Implications for an  
496 intra-Miocene unconformity and paleo-drainage of the proto–Mekong River. *Journal of Sedimentary  
497 Research*, 88(4), 495-515.

498 Hoang, N., and Flower, M. F. J., 1998, Petrogenesis of Cenozoic basalts from Vietnam: Implications for  
499 origins of a Diffuse Igneous Province: *Journal of Petrology*, v. 39, p. 369-395.

500 Huchon, P., Le Pichon, X. and Rangin, C., 1994a. Indochina Peninsula and the collision of India and Eurasia.  
501 *Geology*, v. 22, p. 27-30.

502 Huchon, P., Le Pichon, X., Rangin, C., and Thi, P.T., 1994b. New marine data from Vietnam Margin limit  
503 the amount of extrusion of Indochina during the opening of the South China Sea. AAPG Bull, v. 78.

504 Kasatkin, S.A., Phach, P.V. Anh, L.D. & Golozubov, V.V., 2017. Cretaceous strike-slip dislocations in the  
505 Dalat Zone (Southeastern Vietnam). Russian Journal of Pacific Geology, v. 11 (6) p408-420.

506 Kuiper, K.F., Deino, A., Hilgen, F.J., Krijgsman, W., Renne, P.R., Wijbrans, J.R. (2008) Synchronizing rock  
507 clocks of Earth history, Science v. 325, issue 5875, 500-504. doi: 10.1126/science.1154339.

508 Lee, T.-Y., Lo, C.-H., Chung, S.-L., Chen, C.-Y., Wang, P.-L., Lin, W.-P., Hoang, N., Chi, C. T., and Yem, N. T.,  
509 1998, <sup>40</sup>Ar/<sup>39</sup>Ar Dating Result of Neogene Basalts in Vietnam and its Tectonic Implication, in Flower, M. F.  
510 J., Chung, S.-L., Lo, C.-H., and Lee, T.-Y., eds., Mantle Dynamics and Plate Interactions in East Asia:  
511 Washington, DC, AGU, p. 317-330.

512 Leloup, P. H., Lacassin, R., Tapponnier, P., Schärer, U., Zhong, D., Liu, X., Zhang, L., Ji, S. & Trinh, P. T.  
513 (1995). The Ailao Shan-Red River shear zone (Yunnan, China), Tertiary transform boundary of Indochina.  
514 Tectonophysics, 251(1-4), 3-84.

515 Leloup, P.H., Arnaud, N., Lacassin, R., Kienast, J.R., Harrison, T.M., Phan Trong, T.T., Replumaz, A. &  
516 Tapponnier, P., 2001. New constraints on the structure, thermochronology and timing of the Ailao Shan-  
517 Red River shear zone, SE Asia. Journal of Geophysical Research, v. 106, p. 6683-6732.

518 Lévrier, C., Maluski, H., Van Tich, V., Leyreloup, A., Thi, P. T., & Van Vuong, N. (2004). The early Triassic  
519 Indosinian orogeny in Vietnam (Truong Son Belt and Kontum Massif); implications for the geodynamic  
520 evolution of Indochina. Tectonophysics, 393(1-4), 87-118.

521 Li, C-F., Li, J., Ding, W., Franke, D., Yao, Y., Shi, H., Pang, X., Cao, Y., Lin, J., Kulhanek, D., Williams, T., Bao,  
522 R., Briais, A., Brown, E.A., Chen, Y., Clift, P.D., Colwell, F.S., Dadd, K.A., Hernandez-Almeida, I., Huang, XOL.,  
523 Hyun, S., Jiang, T., Koppers, A.A.P., Li, Q., Liu, C., Liu, Q., Liu, Z., Nagai, R.D., Peleo-Alampay, A., Su, X., Sun,

524 Z., Tejada, M.L.G., Trinh, H.S., Yeh, Y.-C., Zhang, C., Zhang, F., Zhang, G.-L. & Zhao, X., 2015. Seismic  
525 stratigraphy of the central South China Sea basin and implications for neotectonics. *Journal of Geophysical*  
526 *Research*, v. 120, p. 1377–1399.

527 Liu, H.-L., Yan, P., Zhang, B.-Y., Sun, Y., Zhang, Y.-X., Shu, L.-S., Qiu, X.-L., and Guo, L.-Z., 2004, Role of the  
528 Wan-Na fault system in the western Nansha Islands (Southern South China Sea): *Journal of Asian Earth*  
529 *Sciences*, v. 23, p. 221-233.

530 Mantovani, E., Albarello, D., Babbucci, D., Tamburelli, C., and Viti, M., 2002, Trench-arc-backarc systems  
531 in the Mediterranean area: Examples of extrusion tectonics, in Rosenbaum, G., and Lister, G. S., eds.,  
532 *Reconstruction of the evolution of the Alpine Himalayan Orogen.*, Volume 8, p. 125-141.

533 Matthews, S.J., Fraser, A. J., Lowe, S., Todd, S.P., & Peel, F.J., 1997. Structure, stratigraphy and petroleum  
534 geology of the SE Nam Con Son Basin, offshore Vietnam. In Fraser, A.J., Matthews, S.J., & Murphy, R.W.  
535 (eds). *Petroleum Geology of SE Asia*. Geological Society Special Publication 126, p 89-106.

536 Meng, Q. R., Wang, E., & Hu, J. M. (2005). Mesozoic sedimentary evolution of the northwest Sichuan basin:  
537 Implication for continued clockwise rotation of the South China block. *Geological Society of America*  
538 *Bulletin*, 117(3-4), 396-410.

539 Michel, G. W., Yu, Y. Q., Zhu, S. Y., Reigber, C., Becker, M., Reinhart, E., Simons, W., Ambrosius, B., Vigny,  
540 C., Chamot-Rooke, N., Le Pichon, X., Morgan, P., and Matheussen, S., 2001, Crustal motion and block  
541 behavior in SE-Asia from GPS measurements: *Earth and Planetary Science Letters*, v. 187, p. 239-244.

542 Min, K., Mundil, R., Renne, P.R., Ludwig, K.R. (2000) A test for systematic errors in  $^{40}\text{Ar}/^{39}\text{Ar}$   
543 geochronology through comparison with U/Pb analysis of a 1.1-Ga rhyolite. *Geochimica et Cosmochimica*  
544 *Acta*, v. 64, issue 1, 73-98. doi: 10.1016/S0016-7037(99)00204-5.



545 Morley, C. K., 2007, Variations in Late Cenozoic-Recent strike slip and oblique-extensional geometries,  
546 within Indochina: The influence of pre-existing fabrics: *Journal of Structural Geology*, v. 29, p. 36-58

547 Morley, C. K. (2012). Late Cretaceous–early Palaeogene tectonic development of SE Asia. *Earth-Science*  
548 *Reviews*, 115(1-2), 37-75.

549 Nam, T.N., 1995. The geology of Vietnam: A brief summary and problems. *Geoscience reports Shizuoka*  
550 *University* v22, p1-10

551 Nguyen, T. T. B., Satir, M., Siebel, W., & Chen, F. (2004). Granitoids in the Dalat zone, southern Vietnam:  
552 age constraints on magmatism and regional geological implications. *International Journal of Earth*  
553 *Sciences*, 93(3), 329-340.

554 Pubellier, M., & Morley, C. K. (2014). The basins of Sundaland (SE Asia): Evolution and boundary  
555 conditions. *Marine and Petroleum Geology*, 58, 555-578.

556 Rangin, C., Huchon, P., Le Pichon, X., Bellon, H., Lepyrier, C., Roques, D., Hoe, H. D., and Ouynh, P. V., 1995,  
557 Cenozoic deformation of central and south Vietnam: *Tectonophysics*, v. 251, p. 179-196.

558 Redfield, T. F., Scholl, D. W., Fitzgerald, P. G., and Beck, M. E., Jr., 2007, Escape tectonics and the extrusion  
559 of Alaska: Past, present and future: *Geology*, v. 35, p. 1039-1042.

560 Ridgeway, K. D., and Flesch, L. M., 2007, Cenozoic tectonic processes along the Southern Alaska  
561 convergent margin: *Geology*, v. 35, p. 1055-1056.

562 Savva, D., Meresse, F., Pubellier, M., Chamot-Rooke, N., Lavier, L., Po, K. W., ... & Lamy, G. (2013). Seismic  
563 evidence of hyper-stretched crust and mantle exhumation offshore Vietnam. *Tectonophysics*, 608, 72-83.

564 Searle, M.P., Yeh, M-W., Lin, T-H. & Chung, S-L., 2010. Structural constraints on the timing of left-lateral  
565 shear along the Red River shear zone in the Ailao Shan and Diancang Shan Ranges, Yunnan, SW China.  
566 *Geosphere*, v. 6, p. 316-338. DOI: 10.1130/GES00580.1.

567 Shellnutt, J.G., Lan, C.Y., Van Long, T., Usuki, T., Yang, H.J., Mertzman, S.A., Iizuka, Y., Chung, S.L., Wang,  
568 K.L. and Hsu, W.Y., 2013. Formation of Cretaceous Cordilleran and post-orogenic granites and their  
569 microgranular enclaves from the Dalat zone, southern Vietnam: Tectonic implications for the evolution of  
570 Southeast Asia. *Lithos*, 182, pp.229-241.

571 Simons, W.J.F., Socquet, A., Vigny, C., Ambrosius, B.A.C., Haji Abu, S., Promthong, C., Subarya, C., Sarsito,  
572 D.A., Matheussen, S., Morgan, P. and Spakman, W., 2007. A decade of GPS in Southeast Asia: Resolving  
573 Sundaland motion and boundaries. *Journal of Geophysical Research: Solid Earth*, 112(B6).

574 Steiger, R.H. and Jäger, E. (1977) Submission on geochronology: Convention on the use of decay  
575 constants in geo- and cosmochemistry. *Earth and Planetary Science Letters*, v. 36, issue 3, 359-362. doi:  
576 10.1016/0012-821X(77)90060-7.

577 Swiecicki, T. and Maynard, K., 2009. Geology and Sequence, Stratigraphy of Block 06/94, Nam Con Son  
578 Basin, Offshore Vietnam. Proceedings of the 2009 South East Asia Petroleum Exploration Society (SEAPEX)  
579 Conference, p. 1-17.

580 Tapponier, P., Peltzer, G., and Armijo, R., 1986, On the mechanics of the collision between India and Asia,  
581 in Coward, M. P., and Ries, A. C., eds., *Collision Tectonics*, Volume 19, p. 113-157.

582 Tapponier, P., Peltzer, G., Le Dain, A. Y., Armijo, R., and Cobbold, P., 1982, Propagation extrusion tectonics  
583 in Asia: New insights from simple experiments with plasticine: *Geology*, v. 10, p. 611-616.

584 Tingay, M., Morley, C., King, R., Hillis, R., Coblenz, D., Hall, R., 2010, Present-day stress field of Southeast  
585 Asia, *Tectonophysics*, v. 482, 92-104.

586 Trần, Đ. T., Nguyễn, T. Y., Dương, C. C., Vy, Q. H., Zuchiewicz, W., & Nguyễn, V. N. (2013). Recent crustal  
587 movements of northern Vietnam from GPS data. *Journal of Geodynamics*, 69, 5-10.

588 Tri, T.V., Khuc, V. (eds), Tam, B.M., Hoang, C.M., Huyen, D.T., Truong, D.N., Bat, D., Binh, L.D., An, L.D.,  
589 Nhuan, M.T, Toan, N.Q., San, N.T., Minh, N.B., Bieu, N., Dy, N.D., Ty, N.H., Hung, N.Q., Van, N.T., Phong,  
590 N.T., Quy, N.V., Vuong, N.V., Bao, N.X., Luong, P.D., Ngan, P.K., Thien, P., Trinh, P.T., Phuong, T.H., Nam,  
591 T.N., Van, T.T., Thang, T.T., Hai, T.T., Hoa, T.T., Anh, T.T., Long, T.V. & Nghiep, V.C., 2011. Geology and  
592 Earth Resources of Vietnam. Ministry of Natural Resources and Environment, General Department of  
593 Geology and Minerals of Vietnam, Publishing House for Science and Technology, Hanoi. 645pp

594 Trinh, P.T., Van Liem, N., To, T.D., Van Huong, N., Hai, V.Q., Van Thom, B., Van Phong, T., Vinh, H.Q., Xuyen,  
595 N.Q., Thuan, N.V. and Tuc, N.D., 2015. Present day deformation in the east Vietnam sea and surrounding  
596 regions. *Vietnam Journal of Marine Science and Technology*, 15(2), pp.105-118.

597 Uyeda, S., 1994, Heat flow in Vietnam, Circum-Pacific Council Symposium on: Geology, Exploration, and  
598 Development Potential of Energy and Mineral Resources of Vietnam and Adjoining Regions. Abstr.  
599 Program.

600 Van Nguyen, V., & Hoai, L. T. T. (2019). Cenozoic paleostress evolution in south central Vietnam:  
601 Implication for changing dynamics of faulting along the eastern Indochina continental margin. *Journal of*  
602 *Asian Earth Sciences*, 185, 104006.

603 Wang, Y., Fan, W., Zhang, Y., Peng, T., Chen, X., and Xu, Y., 2006, Kinematics and <sup>40</sup>Ar/<sup>39</sup>Ar geochronology  
604 of the Gaoligong and Chongshan shear systems, western Yunnan, China: Implications for early Oligocene  
605 tectonic extrusion of SE Asia: *Tectonophysics*, v. 418, p. 235-254.

606 Yan, P., Deng, H., Liu, H., Zhang, Z., and Jiang, Y., 2006, The temporal and spatial distribution of volcanism  
607 in the South China Sea region: *Journal of Asian Earth Sciences*, v. 27, p. 647-659.

608 Zhou, D., Ru, K., and Chen, H., 1995, Kinematics of Cenozoic extension on the South China Sea continental  
 609 margin and its implications for the tectonic evolution of the region: Tectonophysics, v. 251, p. 161-177.

610 Zhu, M., Graham, S. and McHargue, T., 2009. The red river fault zone in the Yinggehai Basin, South China  
 611 Sea. Tectonophysics, 476(3-4), pp.397-417.

612 Zuchiewicz, W., Quốc Cu'ò'ng, N., Zasadni, J., & Yêm, N. T. (2013). Late Cenozoic tectonics of the Red River  
 613 Fault Zone, Vietnam, in the light of geomorphic studies. Journal of Geodynamics, 69, 11-30.

614

615 **Table 1**

Location #	Latitude (°N)	Longitude (°E)	Elevation (ft)	Brief field description
1	11.4091	107.6399333	788	Quarry in Dambri town, in Jurassic sediments; faulted
2	10.9964	107.1432833	864	Quarry in Soc Lu Formation – basaltic andesite; faulted
3	10.87686667	107.2284	841	Old quarry in alkali basalt; faulted
4	10.38025	107.2564	6	Cretaceous granite outcrop on the coast near Vung Tau; Ca Na-Vung Tau fault zone prominent
5-7	10.38073333	107.2524667	3	Cretaceous granite outcrops on the coast near Vung Tau; subsidiary fault systems to Ca Na-Vung Tau fault zone

8	10.50761667	107.2729167	229	Alkali basalt quarry with xenoliths; jointed but not faulted.
---	-------------	-------------	-----	---------------------------------------------------------------

616

617 Table 1: Co-ordinates and brief field descriptions for the locations referenced in this study. Co-ordinates  
618 are given in decimal degrees and in WGS 84 convention. Elevations are given in feet above sea level.

619

620

621

622

623

624

625

626

627

628

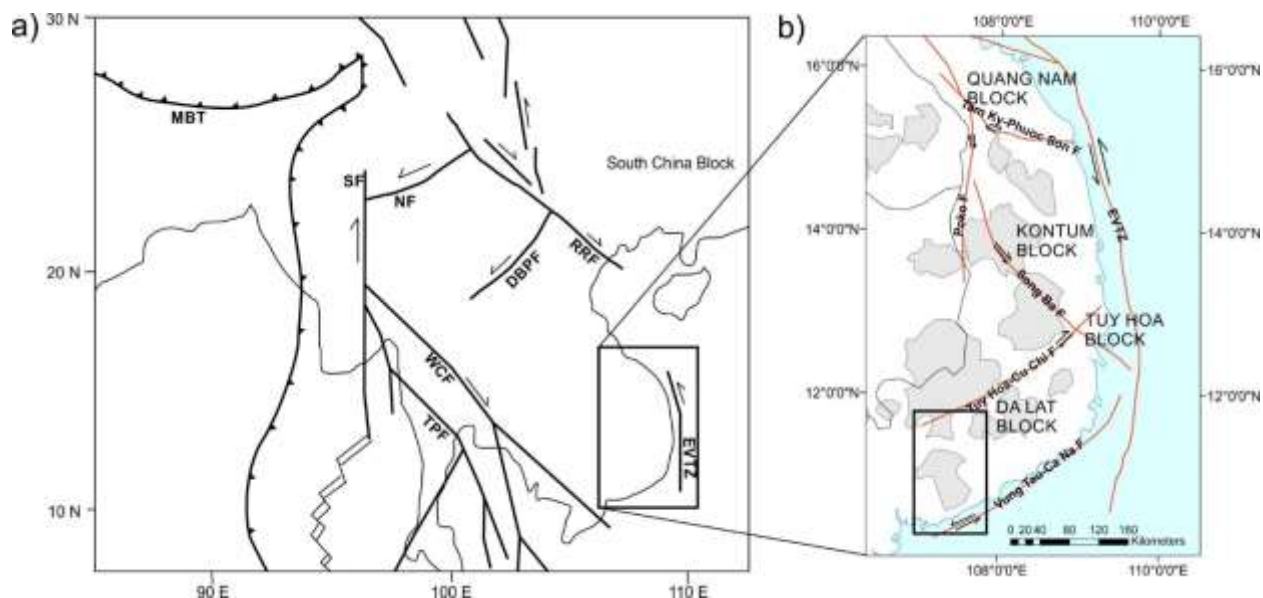
629

630

631

632

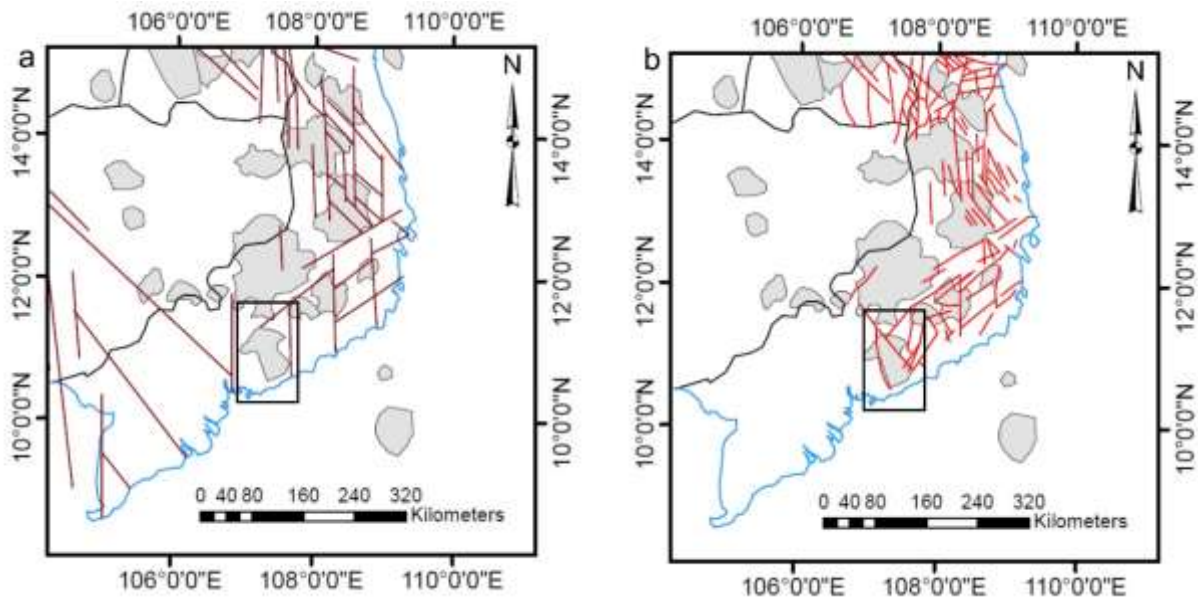
633 Figure 1



634  
 635 Tectonic maps of the region. a) shows regional faults of the Himalayan orogen as well as the major  
 636 strike-slip faults of the Indochina Peninsula, modified after Leloup et al. (1995) and Nam (1995). MBT,  
 637 Main Boundary Thrust; SF, Sagaing Fault; NF, Nanting Fault; TPF, Three Pagodas Fault; WCF, Wang Chao  
 638 Fault; EVTZ, East Vietnam Transfer Zone; RRF, Red River Fault; DBPF, Dien Bien Phu Fault. b) Block map  
 639 of the wider study area after Kasatkin et al. (2017). Red lines mark faults, grey areas are volcanic  
 640 centers. Black box marks the present detailed study area.

641  
 642  
 643  
 644  
 645  
 646  
 647  
 648  
 649  
 650  
 651  
 652  
 653

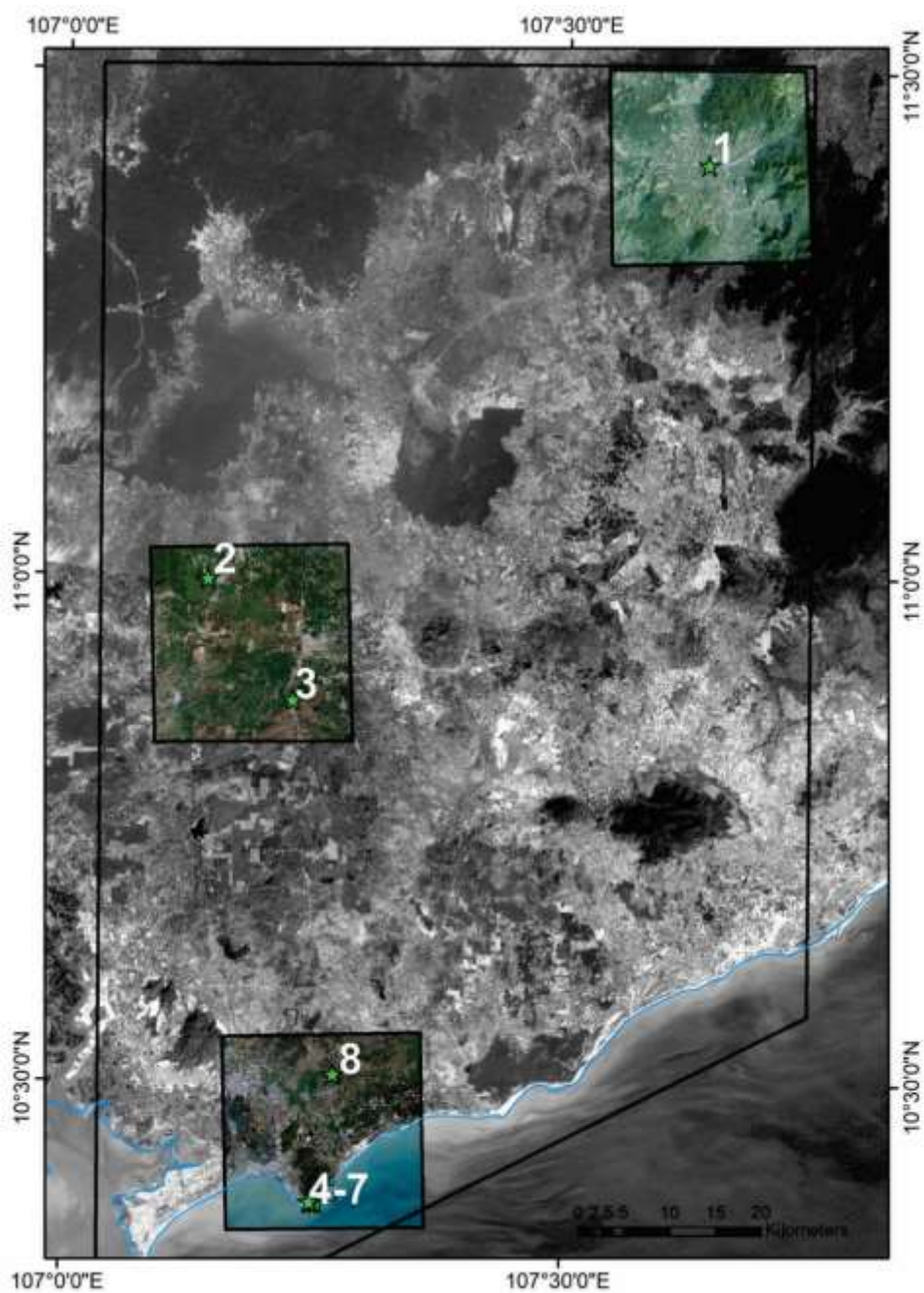
654 Figure 2:



655  
656 Contrasting fault maps for the Da Lat block and southern part of the Kontum block. a) is from Huchon et  
657 al. (1994a), and shows their interpretation of the Paleogene fault framework in the region. b) is from  
658 Rangin et al. (1995) and shows their contrasting interpretation of the dominant fault patterns in the  
659 area. Grey areas are volcanic centers and the black box marks the location of the present study area.

660  
661  
662  
663  
664  
665  
666  
667  
668  
669  
670  
671  
672

673 Figure 3:



674

675 Landsat ETM+ coverage of the study area, in greyscale, showing field locations (green stars with white  
676 numbers) and locations of the SPOT patches used for detailed analysis of key areas (colored squares of  
677 higher resolution imagery).

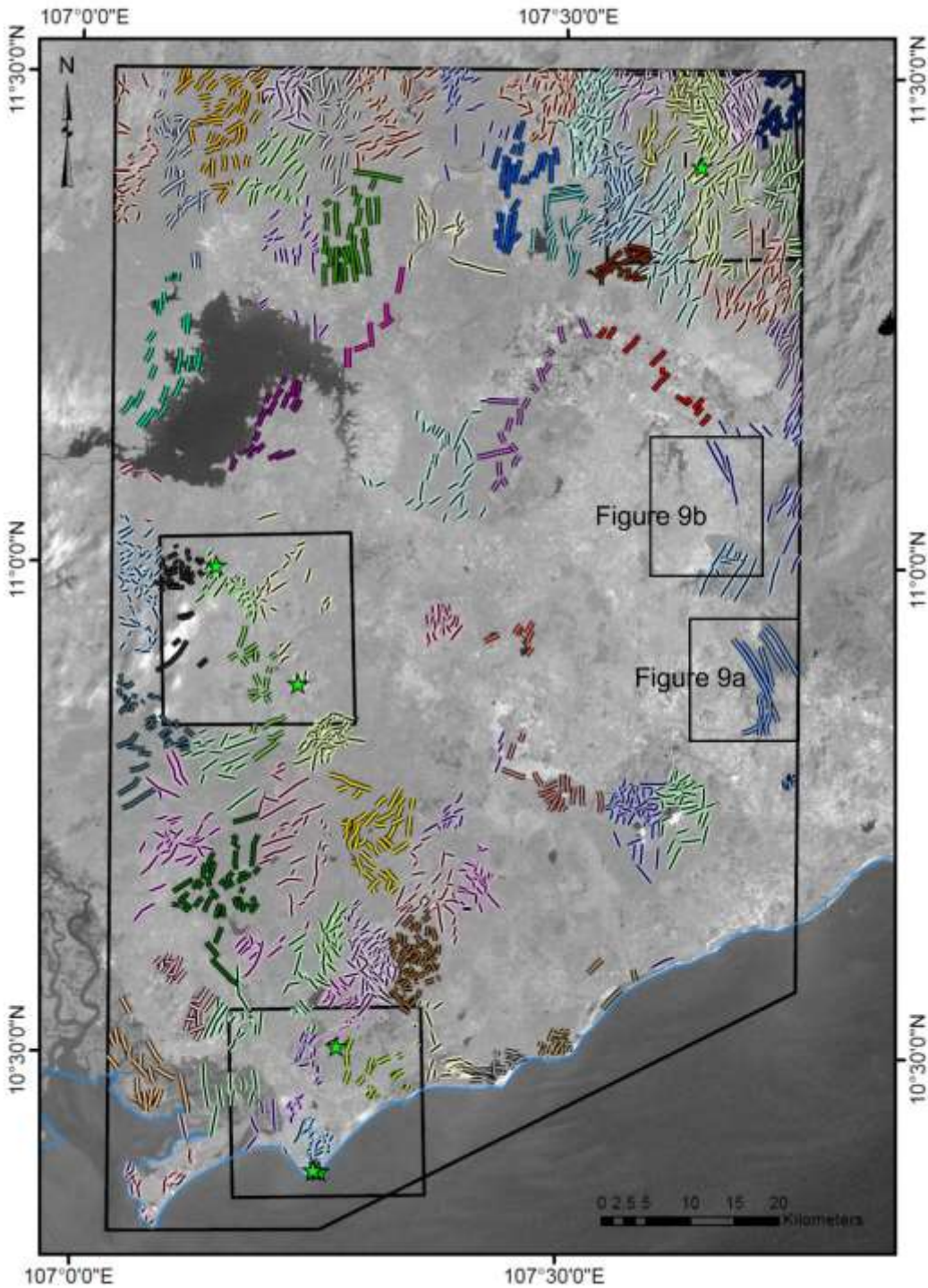
678

679

680

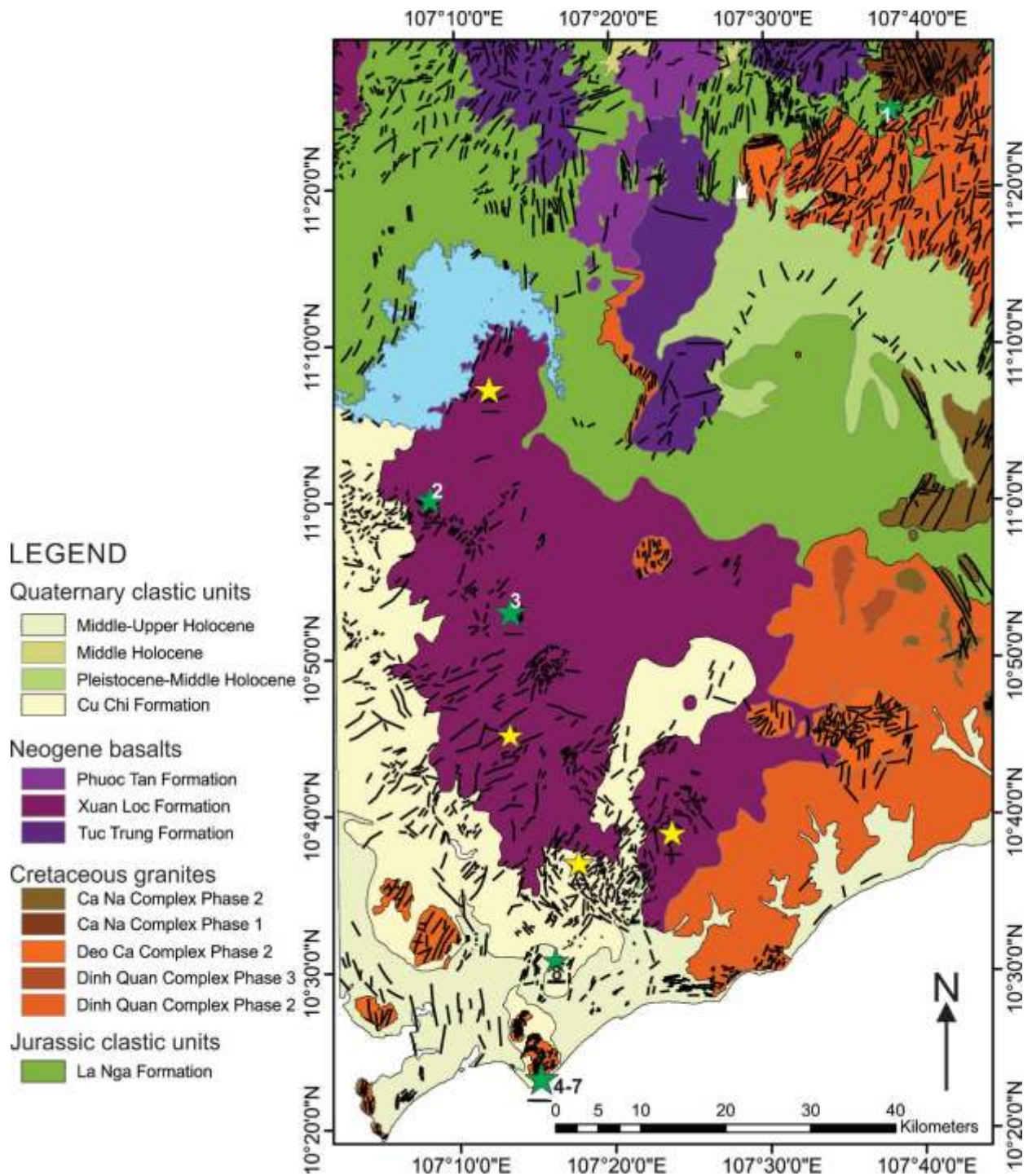


681 Figure 4:



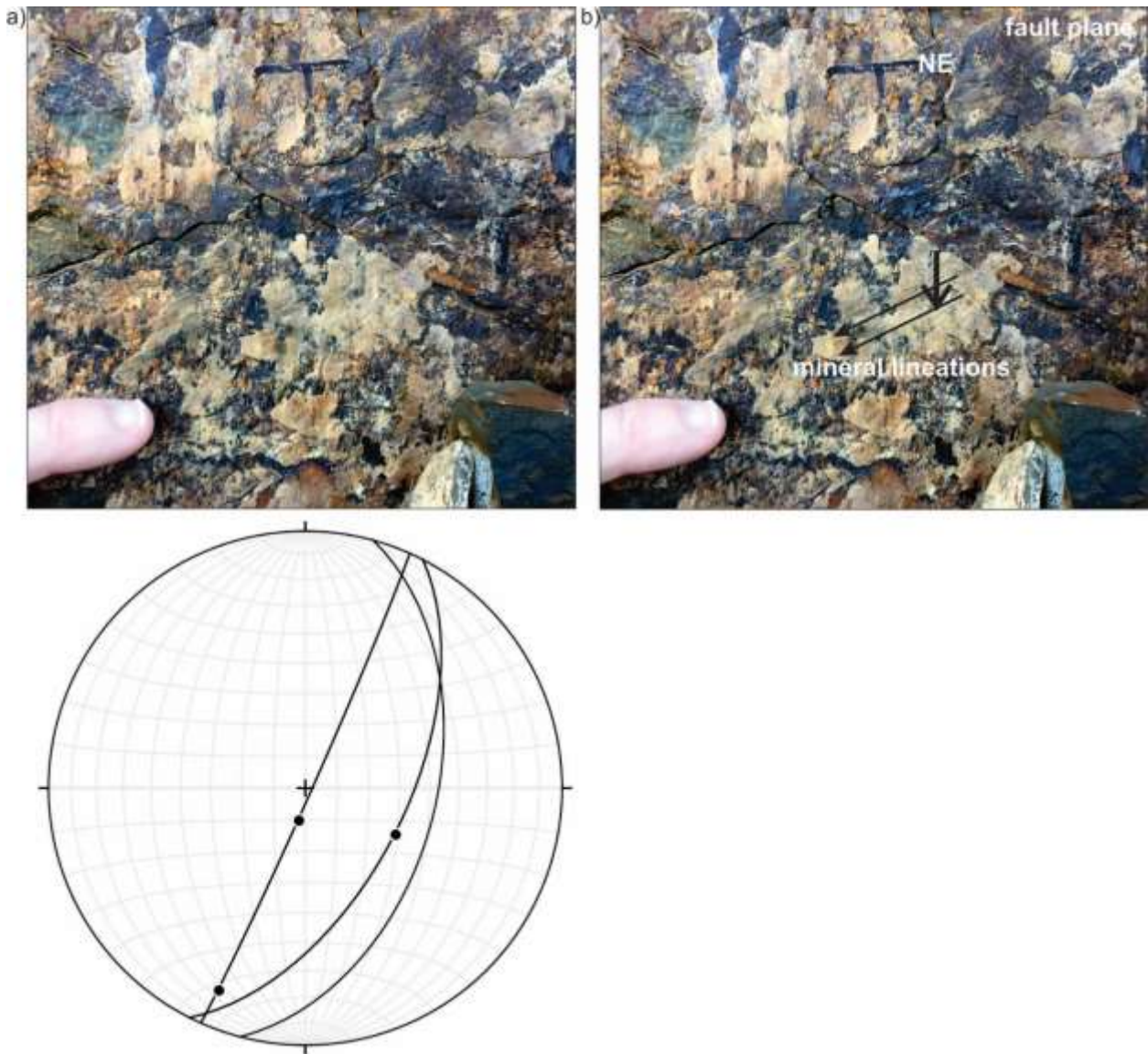
682

683 Classified lineaments across the study area, superimposed on a Landsat ETM+ image. Lineaments have  
684 been classified into 75 bins based on a nearest neighbor algorithm in the ArcGIS Grouping Analysis. Black  
685 boxes show the location of SPOT datasets. Green stars represent the locations visited in the field, with  
686 location numbers as in Figure 3. The location of Figure 13a and Figure 13b are also shown.



688

689 Geologic map of the study area showing that lineaments cut both young (Neogene) and older  
 690 (Cretaceous-Jurassic) formations. Numbered green stars mark field locations from this study. Yellow  
 691 stars mark locations with previously dated basalts (either from outcrop or from core) from Lee et al.  
 692 (1998) ranging in age from  $2.42 \pm 0.08$  Ma in the south, to  $0.24 \pm 0.06$  Ma in the north of the Xuan Loc  
 693 Formation. Basalts at location 2 have been previously dated by An et al. (2017) to be  $4.3 \pm 0.2$  Ma.



695

696

697 a) Field photograph showing fault plane with mineral lineations in the Jurassic sediments at location 1.  
698 b) Annotated version of image in part (a); black arrows show orientations of mineral lineations, where  
699 the longer arrows cross-cut the shorter, dip-slip arrow. c) stereonet with great circles indicating fault  
700 planes, and dots indicating lineations on fault planes where observed. The stereonet shows all faults  
701 present at this location. The near-vertical fault plane with two lineations is the fault plane shown in  
702 parts a and b.

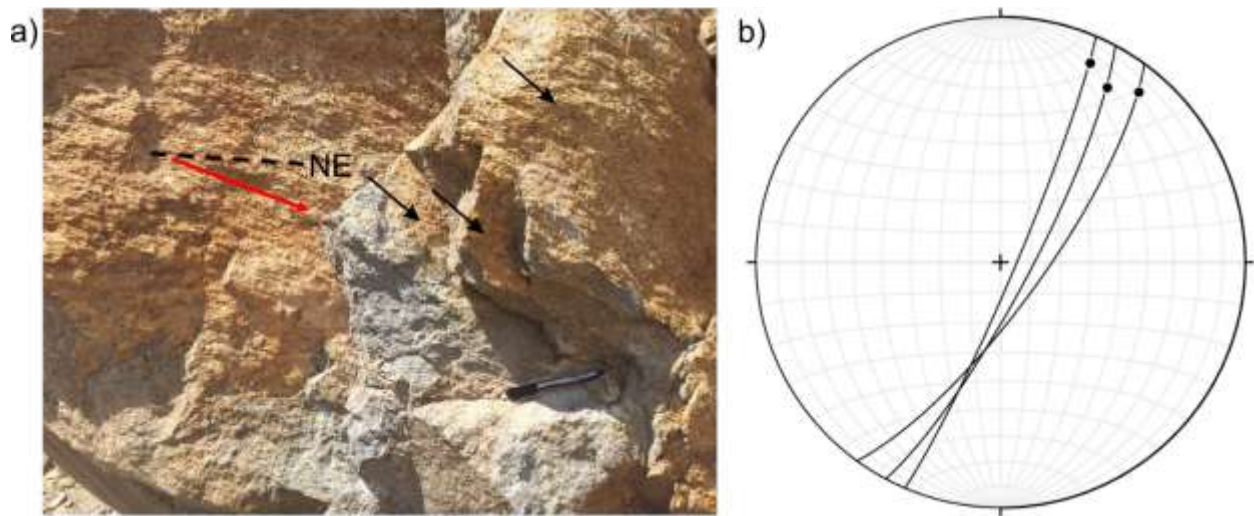
703

704

705

706

707 Figure 7



708

709 a) Faults in the Pliocene Soc Lu Formation, at location 2. The black dashed line shows the strike of the  
710 fault, and the red arrow shows the trend and plunge of the lineations on one fault plane. Other fault  
711 planes are arrowed. b) Stereonet as for Figure 6, showing fault planes and lineations recorded at this  
712 location. Note the lack of dip-slip lineations and the prevalence of strike-slip lineations.

713

714

715

716

717

718

719

720

721

722

723

724

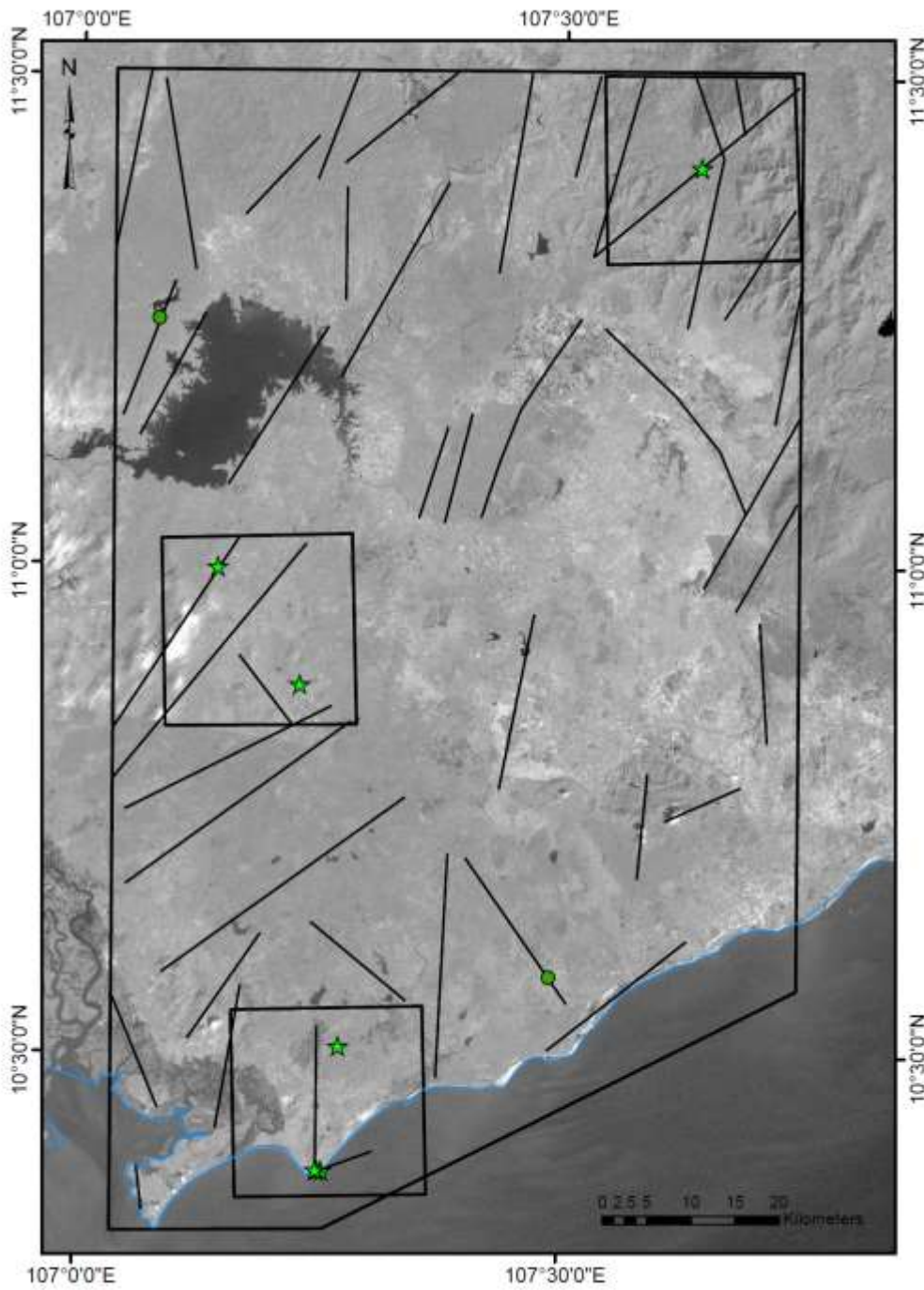
725

726

727

728

729 Figure 8



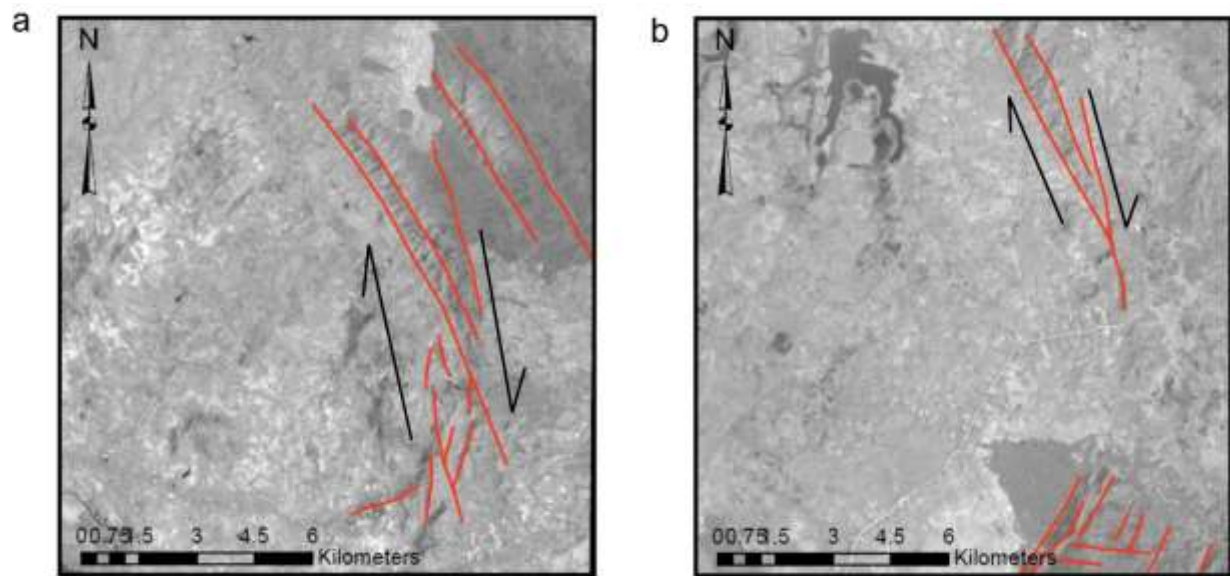
730

731 Post-Jurassic, pre-Neogene fault map of the study area, derived from the classified lineaments. Black  
732 boxes show the location of SPOT datasets. Green stars represent the locations visited in the field, with  
733 location numbers as in Figure 3. Green dots represent the locations of known earthquakes.

734

735

736 Figure 9



737

738 Examples of lineament patterns developing above a reactivated strike slip fault. For the location of each  
739 of these examples, see Figure 4.

740

741

742